Effect of Plasma Processing Gas Composition on the Nitrogen-Doping Status and Visible Light Photocatalysis of TiO_2

Chienchih Chen,[†] Hsunling Bai,*[,†] and Chungliang Chang[‡]

Institute of Environmental Engineering, National Chiao Tung University, 75 Po-Ai Street, Hsinchu, Taiwan, and Department of Environmental Engineering and Health, Yuanpei Institute of Science and Technology, Hsinchu, Taiwan

Received: February 27, 2007; In Final Form: August 5, 2007

The atmospheric pressure plasma enhanced nanoparticle synthesis (APPENS) process is applied to produce nitrogen (N) doped titania (TiO_2) photocatalysts. With TTIP (titanium tetraisopropoxide; $Ti(OC_3H_7)_4$) and water vapors as precursors, the effect of plasma and annealing gas composition on the N-doping status is identified by a cross comparison of the chemical shift of N atoms with those of Ti and O atoms. The activities of various types of N-doped photocatalysts are evaluated via the conversion of isopropyl alcohol (IPA). The results show that the N-doped TiO_2 particles with O_X-Ti-N_Y and −(NO) dopants are produced via N_2 plasma gas followed by air or N_2 annealing gases. They have better visible and UV photocatalytic activities compared to the pure TiO_2 photocatalysts prepared under O_2/Ar plasma and annealing gases. On the other hand, the N-doped TiO_2 photocatalyst produced under N_2/O_2/Ar plasma gas and then annealed with pure N_2 gas tends to have an additional dopant of $-(NO_2)$, but its photocatalytic activity is even worse than those of the pure TiO_2 photocatalysts. The results reveal that the O_X-Ti-N_Y and −(NO) dopants may have positive effects on the visible light photocatalytic activity while the $-(NO_2)$ dopant tends to have a negative effect on the visible light photocatalytic activity.

1. Introduction

The TiO_2 photocatalysts have been extensively studied owing to their chemical stability and wide applications to environmental pollution control.[1] However, the pure TiO_2 photocatalysts can be effectively utilized under UV (λ < 365 nm) light source only. Thus the development of visible light photocatalysts has received wide attention in order to enhance the utilization rate of solar energy. The modified TiO_2 that utilizes a visible light source can be achieved[2−4] by doping with various elements such as metals, F, S, N, etc.

Nitrogen-doped TiO_2 has been recognized as one of the most effective means for band gap narrowing via mixing of the 2p state of substituted N with the 2p state of O in TiO_2 lattice.[4] The sources of N-doping can be N_2 gas, ammonium chloride, ammonia gas, or other N-containing compounds,[4−9] and they are doped into TiO_2 photocatalysts to enhance photocatalytic activity in the visible light range.[4−21]

Up to the present, many methods have been documented to successfully prepare N-doped TiO_2 films or particles, including surface treatment of TiO_2 target by sputtering[4] or plasma,[10] manufacturing from TiO_2 precursors via the plasma-enhanced chemical vapor deposition (PECVD) process,[8] pulse laser deposition,[11] the ion-assisted electron beam evaporation method,[12] and aqueous phase reactions such as the sol−gel method.[13−17] Most of the studies on N-doped TiO_2 commonly utilized XPS (X-ray photoelectron spectroscopy) for the characterization of N atoms present in TiO_2, but the N-doping status was frequently reported as $TiO_{2-x}N_x$ without specifying the actual N-doping status of the N impurity.

The atmospheric pressure plasma enhanced nanoparticle synthesis (APPENS) process developed by the present authors,[19] regarded as one of the PECVD processes except that it is operated under atmospheric pressure and temperature, can be used for the production of N-doped TiO_2 particles. In this study, $TiO_{2-x}N_x$ nanoparticles of near-uniform size are produced by the APPENS process. The N-doping status is varied by changing the carrier gas compositions under plasma and annealing atmospheres. The N-doping statuses of the photocatalysts are speculated by a cross comparison of the chemical shifts of Ti, O, and N atoms observed from the XPS data. The effects of plasma and annealing gas compositions on the binding energies of Ti, N, and O and on the activities of N-doped photocatalysts in terms of isopropyl alcohol (IPA) conversion are identified under both UV and visible light sources.

2. Core Level Binding Eneries of Ti, N, and O in N-Doped TiO_2

Although it has been widely accepted[6,8−11,13,15] that TiN doping in TiO_2 photocatalyst has a positive effect on the visible light photocatalytic activity since the report of Asahi et al.,[4] there are still other types of N-doping existing such as −(NO), $-(NO_2)$, and (O−Ti−N).[13,14,16−18,20,21] Nosaka et al.[13] doped N atoms into commercial TiO_2 particles with organic compounds and observed the presence of TiN and −(NO) in the photocatalysts. They indicated that both TiN and −(NO) doping in TiO_2 contributed to visible light absorbance. However, TiN tended to increase the visible light photocatalytic activity while −(NO) doping had a negative effect on visible light photocatalytic activity.

However, Sato et al.[14] and Yin et al.[15] prepared N-doped anatase TiO_2 powders and obtained −(NO) doping as the only

* Corresponding author. Fax: +886-3-5725958.E-mail: hlbai@mail.nctu.edu.tw.
[†] National Chiao Tung University.
[‡] Yuanpei Institute of Science and Technology.

10.1021/jp0716233 CCC: $37.00
Published on Web 10/03/2007

TABLE 1: Literature Data on the Core Level Binding Energies (eV) of Ti 2p, N 1s, and O 1s[4,6,8−10,13−16,18,20,21,25−33]

species	assigned doping status
Ti $2p_{3/2}$, 455.0−459.5	TiN (455.2 ± 0.2,[27] 455.6,[25] 455.9 ± 0.2[26])
	TiN_XO_Y (455.2[29])
	$TiO_{2-x}N_X$ (456−459,[10] 459.1[8])
	titanium oxynitride (456.5[31])
	oxidized TiN (456.8[27])
	TiO_2 (458.5,[29] 458.8,[25,31] 458.8 ± 0.34,[26] 459.1[27])
Ti $2p_{1/2}$, 461.0−465.0	TiN_XO_Y (461[29])
	oxidized TiN (462.6[27])
	$TiO_{2-x}N_X$ (464.4,[8] 463−465[10])
	TiO_2 (464.34,[26] 464.4,[29] 464.7[31])
N 1s (I), 395.8−397.8	$TiN_{X>1}$ (395.85[29])
	TiN (396,[4,6,10,13,15,27] 396.1,[8] 396.5,[18] 396.6,[25] 396.7,[20] 397,[28] 397.2 ± 0.5,[26] 397.8[25])
	TiN_XO_Y (397[29])
N 1s (II), 398.8−401.2	N−C, N−O, NN (399.25,[29] 400,[9,10,13−15,29,32] 398.8−400.3,[28] 398.9 ± 0.8[26])
	molecularly chemisorbed γ-N_2 (399.3,[8] 400,[4,9,27] 401.15[29])
	nitrogen contaminant (398.8−400.3[28])
	Ti−N−O (399.5[18])
	interstitially dopant N−H (399.6[20])
	Ti−O−N (400[14,16])
N 1s (III), 402.0−403.3	O−Ti−N (402[21])
	molecularly chemsorbed γ-N_2 (402[4,27])
	oxidized TiN (N_X−Ti−O_Y; 402−403.3[25])
	NO_X (402.5[30])
N 1s (IV), 403.9−404.3	−NO_2 (404,[32,33] 404.1 ± 0.2[26])
O 1s (I), 528.1−531.1	metal oxide (529.6 ± 1.5[26])
	TiO_2 (529.7,[29] 530 ± 0.2,[27] 530.2,[18] 530.5[25])
	TiN_XO_Y (531[29])
O 1s (II), 531.4−532.4	substoichiometric oxide, oxynitride (531.4[27]), Ti−N−O (532[18]), O−Ti−N (532[21]), adsorbed oxygen (532.2[25])
	OH (532.4[29])
O 1s (III), 532.7−533.7	−NO_2 (533.2 ± 0.5[26])
	CO (533.4[29])

status of N-doped TiO_2. Their results showed that the presence of −(NO) at N 1s binding energy of around 400 eV is an effective N-doping site. Diwald et al.[20] also showed that the peak observed at 399.6 eV is responsible for the shift of the photochemical threshold down to ∼2.4 eV. Also, this form of nitrogen is most likely located in an interstitial site bound to hydrogen. Diwald et al.[20] indicated that this form of N-doping disagrees with the conclusion of Asahi et al.[4] A similar observation was shown by Chen et al.[16,21] that TiO_2 with oxynitride doping at N 1s binding energy of around 402 eV is an effective photocatalyst in the decomposition of methylene blue.

The visible light induced photocatalytic activity may also be due to the presence of localized N 2p states.[22−24] Di Valentin et al.[22] observed that N-doping has opposite effects on the photoactivity of anatase and rutile TiO_2 because of different structures and densities, leading to a red shift and a blue shift, respectively, of the absorption band edge. In both cases the doping is accompanied by the appearance of well-localized N 2p states above the O 2p valence band, but in rutile the shift of the top of the valence band toward lower energies leads to an increase of the band gap transition.

It must be noted that the binding energy of XPS data is binding of electron in the atom, not binding between atoms. Thus, one cannot directly assign a chemical binding between the Ti, O, and N atoms by the presence of a given peak in the XPS spectra. The other atoms surrounding the Ti atom might influence the charge of Ti. Thus, in this study the N-doping status of TiO_2 was first proposed by comparing the chemical shift of elements with the XPS handbook[26] and the literature[4,6,8,9,12−16,18,20,21,25−33] and then confirmed by cross comparison of the chemical shifts of Ti 2p, O 1s, and N 1s atoms.

Table 1 lists the binding energies of Ti 2p, N 1s, and O 1s obtained from the XPS Handbook[26] as well as literature data on N-doped TiO_2 photocatalysts[4,6,8,9,12−16,18,20,21,25−33] or other nitrogen impurity materials.[32,33] Although there might be some differences in the values of the binding energies of Ti 2p, N 1s, and O 1s as detected by different instruments and laboratories, they can still be identified as TiO_2 and TiN at $2p_{3/2}$ and $2p_{1/2}$, and be grouped into several ranges as N(I)−N(IV) for N 1s and O(I)−O(III) for O 1s.

The Ti 2p binding energies of Ti $2p_{3/2}$ (455.0−459.5 eV) and Ti $2p_{1/2}$ (461.0−465.0 eV) were different for TiO_2 and TiN. The core level binding energy of Ti 2p of TiN tended to be lower than that of TiO_2. The group I of N 1s spectra with peaks at 395.8−397.8 eV indicated that the N-doping status was TiN as indicated in Table 1, while those of N(II)−N(III) around 399−403 eV revealed the presence of N_2 chemisorption or the oxynitride doping such as Ti−N−O, Ti−O−N, N_X−Ti−O_Y, and O−Ti−N. For N(IV) there existed an additional N-doping status of −(NO_2) in TiO_2 particles. The binding energy of O(I) with peaks at 528.1−531.1 eV shows that the O atom was bound to metals such as Ti, while for O(II) and O(III) the O atom was bound to N or other atoms such as C and H. The binding energies of Ti 2p, N 1s, and O 1s listed in Table 1 will be used hereafter as references for cross identification of the status of N-doped TiO_2 particles produced in this study.

3. Experimental Section

Figure 1a shows the experimental setup of the reactor for synthesizing the photocatalysts. The precursors for producing photocatalysts were TTIP (titanium tetraisopropoxide; $Ti(OC_3H_7)_4$) and deionized water. They were vaporized and sent into the plasma reactor (i.e., the APPENS reactor) via passing the carrier gases through two series of impingers controlled at temperatures of 150 and 25 °C, respectively, for TTIP and water. The carrier gas compositions ($Ar/N_2/O_2$) were controlled by mass flow

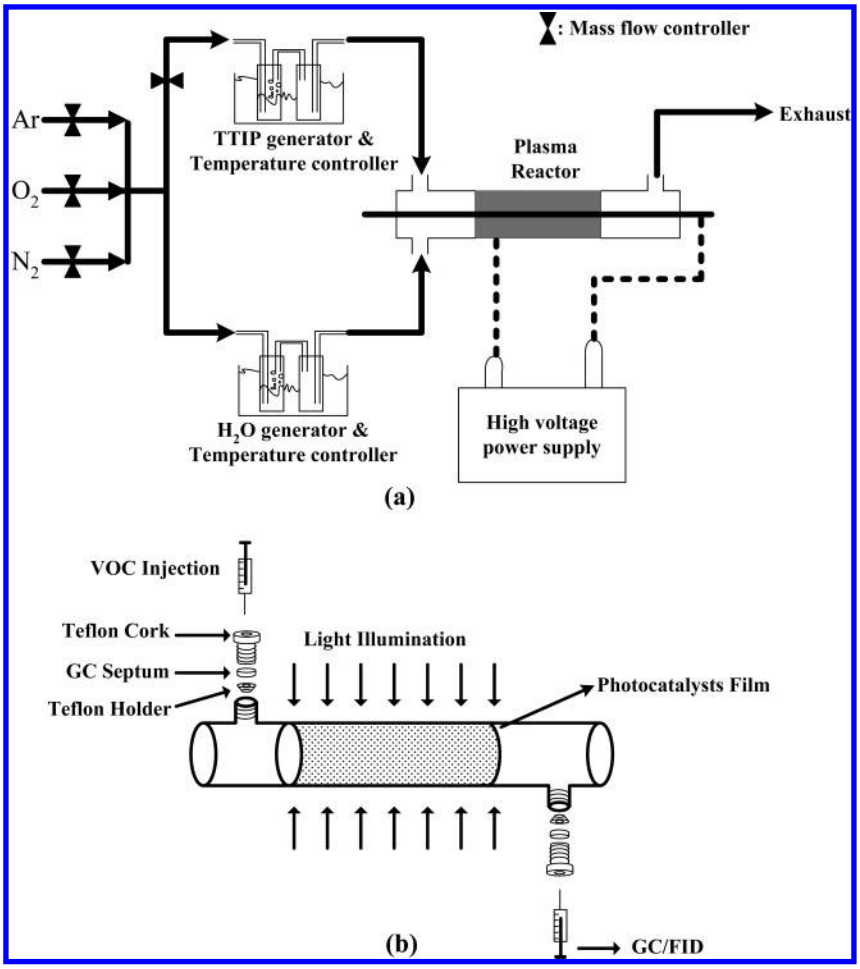

Figure 1. Schematic diagrams of (a) APPENS reactor for producing N-doped TiO_2 photocatalysts and (b) batch type photocatalytic reactor for IPA removal.

TABLE 2: Plasma and Annealing Gas Compositions for Synthesizing Different TiO_2-Based Photocatalysts

photocatalysts	plasma gas	anneal gas
SYN1	100% N_2	air (20% O_2 + 80% N_2)
SYN2	100% N_2	20% N_2 + 80% Ar
SYN3	20% O_2 + 80% Ar	20% O_2 + 80% Ar
SYN4	10% N_2 + 10% O_2 + 80% Ar	20% N_2 + 80% Ar

controllers (Brooks, 5860E). The total flow rate of precursor vapors was 150 cm^3/min with a TTIP/H_2O volumetric flow rate ratio of 1.0.

The main part of the APPENS reactor was made of Pyrex with a 21 mm inner diameter and a 23 mm outer diameter. It was based on a tube-line type glow dielectric barrier discharge reactor. One electrode was a stainless rod of 2 mm in diameter and located along the central line of the reactor. The other electrode was stainless steel mesh wrapped around the reactor of 135 mm in length. Alternating current (ac) with 60 Hz frequency was applied to the APPENS reactor. The reactor was operated at 9.6 kV/cm electric field strength and atmospheric pressure conditions. The carrier gases of N_2 or O_2 molecules were excited in the nonthermal plasma environment and N atoms or N-containing molecules were implanted into the TiO_2 vapor precursors or particles. The product particles were deposited on the inner surface of the reactor for further photocatalytic activity testing and particle characterization.

Table 2 shows synthesized gas compositions for obtaining different types of N-doping in the TiO_2 particles. The four tests were conducted under different plasma and annealing gas compositions, and the photocatalysts produced under the four tests are denoted SYN1−SYN4 hereafter. After 10 h of the plasma process, the product particles were then annealed at 500 °C for 3 h with a gas flow rate of 10 cm^3/min. SYN1 and SYN2 were processed under the same plasma gas environment composed of pure N_2 gas, and then SYN1 was annealed in an air environment while SYN2 was annealed with 20% N_2 + 80% Ar gases. SYN3 was produced without the presence of N_2 gas for the purpose of producing pure TiO_2 particles without any N-doping. It was processed in a 20% O_2 + 80% Ar plasma and annealing gas environment. The plasma gases for producing SYN4 were 10% N_2 + 10% O_2 + 80% Ar, and the annealing gases were 20% N_2 and 80% Ar.

After annealing, the elements and N-doping status of TiO_2 particles were analyzed by XPS (Perkin-Elmer, Phi 1600). The crystal phase of collected particles was characterized by XRPD (X-ray powder diffraction; Rigaku) with a Cu target at 30 kV, 20 mA. The result of the XRPD analysis was compared to JCPDS (Joint Committee on Powder Diffraction Standards) for crystal characterization. The morphology of product particles was observed in the SEM (scanning electron microscope; HITACHI-S4700) images. The UV−visible diffuse reflection spectra were measured by a spectrophotometer (U-3010, Hitachi) with a 60 mm integrating sphere.

The photocatalytic activities of photocatalysts obtained from SYN1−SYN4 were tested for their IPA conversion with a batch type reactor. The batch photocatalytic reactors were the same

as those used for producing TiO_2 catalytic particles during the APPENS process. Figure 1b is a schematic diagram of the batch photocatalytic reactor for IPA conversion. The inlet and outlet of reactors were sealed to form a batch type configuration. A fixed amount of IPA was injected into the sealed reactor and evaporated under a constant temperature of 45 °C and relative humidity of 70%.

The IPA reached a steady-state vapor concentration of 100 ± 5 ppm after about 60 min as confirmed by a gas chromatograph/flame ionization detector (China Chromatography, 9800). Considering that different superficial properties of the SYN1−SYN4 photocatalysts may affect adsorption,[34] the quantity of IPA adsorbed by each photocatalyst was tested in this study. After the injected IPA reached a steady-state concentration in the reactor, the adsorption quantity was calculated to be 1.22, 1.24, 1.25, and 1.24 $\mu g/mg_{catalyst}$, respectively, for SYN1, SYN2, SYN3, and SYN4 photocatalysts. Therefore, the influence of absorption among different photocatalysts can be neglected in this work.

Once the steady-state concentration of IPA was reached, the light was turned on and the IPA vapors were sampled and analyzed for their concentrations. To avoid the diffusion limitation in a batch reactor, the light was turned off again for 30 min after each sampling to ensure good mixing of the IPA molecules; then the light was turned on again to continue the photocatalysis tests. The illumination light sources used in the batch photocatalytic decomposition studies were either UV (364.2 nm; FL10BLB, Sankyo Denki) or visible light (major peaks at 435, 488, 545, 587, and 611 nm; FL10D-EX, Tyo Light) sources of cylindrical lamps having the same irradiation intensity (10 W). Both the intensity and the spectra of the light sources were obtained from a spectrophotometer (Ocean Optics, USB2000). The intensities of illumination in the reactor were 3.78 mW/cm^2 for the UV light source and 4.81 mW/cm^2 for the visible light source.

To facilitate understanding of the prepared photocatalyst for indoor air pollution control application, the visible light lamp used in this study was simply the one used in household living space. There was a very small peak in the UV range of 364 nm with an intensity of 0.35 mW/cm^2 for the visible light source. To evaluate the effect of this small peak at 364 nm on visible light photocatalysis, a photocatalysis test was conducted with a UV source (364.2 nm) of 0.43 mW/cm^2 intensity (precise control of the light intensity to be 0.35 mW/cm^2 was not feasible during the test). The result revealed that the IPA conversion concentration was below the detection limit. In addition, blank tests were also conducted including those with catalyst but without illumination, and those without catalyst but with light illumination. Each type of blank test showed that the conversions of IPA were negligible.

4. Results and Discussion

4.1. IPA Conversion. The photocatalytic activities of SYN1−SYN4 samples obtained under different synthesized gases were tested via IPA conversion, and the results are shown in Figures 2 and 3, respectively, with visible and UV light sources. It is observed in Figure 2 that all types of TiO_2 particles including the pure TiO_2 photocatalyst produced via SYN3 have some IPA conversion under visible light. Because prior photocatalytic tests with a 364.2 nm UV lamp at the intensity of 0.43 mW/cm^2 showed negligible photoactivity, it was confirmed that the photoactivity was not due to the minor UV peak (0.35 mW/cm^2 at 364 nm) of the visible light source. A similar observation

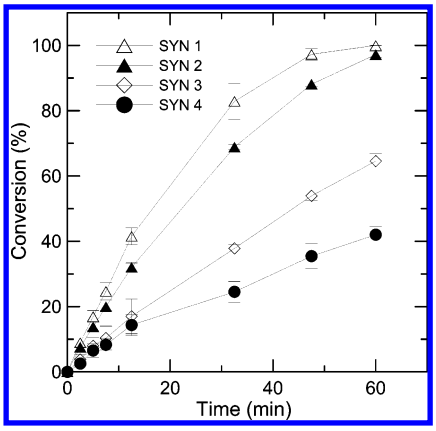

Figure 2. IPA conversion under visible light source (435, 488, 545, 587, and 611 nm, 10 W) at 45 °C with a batch type photocatalytic reactor.

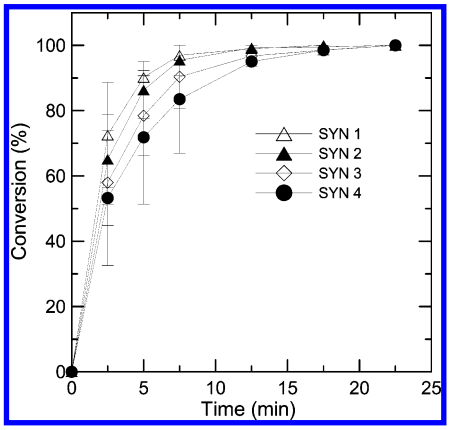

Figure 3. IPA conversion under UV light source (364.5 nm, 10 W) at 45 °C with a batch type photocatalytic reactor.

was found in the literature: for example, Asahi et al.[4] and Nosaka et al.[13] used color filters to filter out the UV light source and then conducted photocatalytic tests in the visible light range for pure anatase TiO_2; they still obtained some photoactivity. Livraghi et al.[24] and Huang et al.[34] also had similar results: they attributed the phenomena to surface absorption or the oxygen vacancy.

The photocatalytic activities in terms of IPA conversion are in the order SYN1 > SYN2 > SYN3 > SYN4 under both visible and UV light sources as observed in Figures 2 and 3. The difference in the IPA conversion is especially significant for the visible light test results as shown in Figure 2, where complete removal of IPA can be achieved after around 60 min for SYN1, but for SYN4 the IPA conversion was only around 40%. The SYN4 photocatalyst has less IPA conversion than the pure TiO_2 particles of SYN3. The observations indicated that the N-doped TiO_2 photocatalyst may not necessarily have a higher photocatalytic activity under the visible light source. Because the photocatalytic activity of TiO_2 particles may be affected by many factors such as particle size, crystal phase, UV−visible light absorption spectra, and the N-doped status,[4−21] these factors are discussed in the following.

4.2. Crystallite and Particle Size. SEM images are shown in Figure 4 for SYN1−SYN4 photocatalysts. It is observed that the photocatalytic particles synthesized under 100% N_2 plasma environment (SYN1 and SYN2) seem to be larger than those under 20% O_2 (SYN3) and 10% N_2+ 10% O_2 + 80% Ar (SYN4) plasma environment. The particle sizes of SYN1 and SYN2 are around 50 nm, as roughly estimated from the SEM

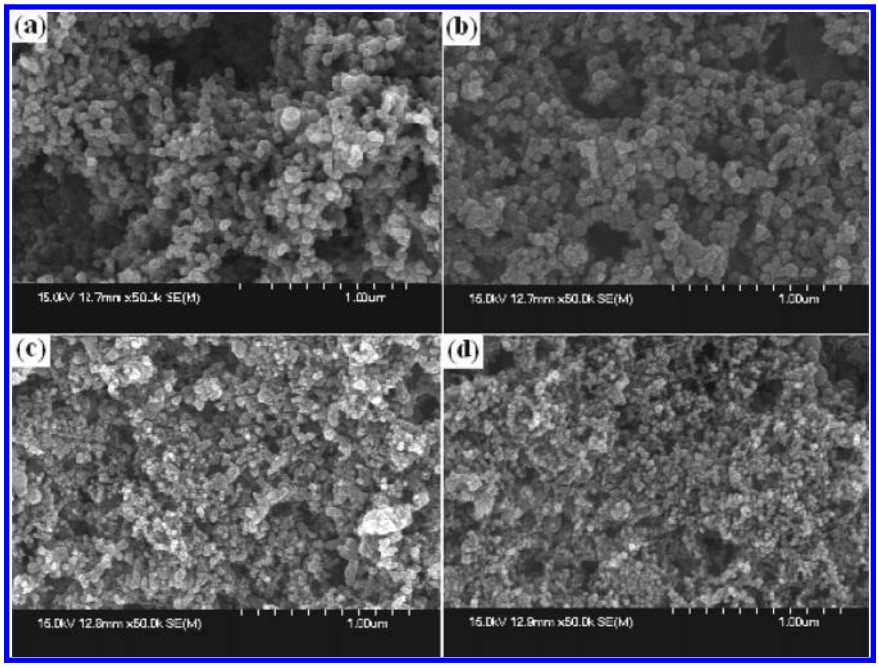

Figure 4. SEM images of particles produced via (a) SYN1, (b) SYN2, (c) SYN3, and (d) SYN4.

TABLE 3: Crystallite Sizes of SYN1−SYN4 Photocatalytic Particles[a]

photocatalyst	max peak (2θ)	fwhm (β)	crystallite size (D, nm)
SYN1	25.23	0.006 53	21.76
SYN2	25.28	0.006 67	21.30
SYN3	25.38	0.006 13	23.18
SYN4	25.36	0.006 53	21.76

[a] The crystallite sizes were calculated based on the Scherrer equation with parameter values obtained from XRPD patterns (X-ray wavelength (λ) was 0.154 056 nm).

images. They are around 25 nm for SYN3 and SYN4. Calculating the crystallite size of particles (D, nm) from the Scherrer equation[35] using the XRPD measurement data

$$D = \frac{0.9\lambda}{\beta \cos \theta}$$

where λ (nm) is the X-ray wavelength for the XRPD test, θ is the Bragg angle, and β is the full width of diffraction at half of maximum intensity (fwhm), it was obtained that the crystallite sizes for SYN1−SYN4 are about the same around 22.0 ± 1.2 nm as listed in Table 3. Therefore, one can conclude that the primary crystallite particle size of SYN1 and SYN2 is the same as that of SYN3 and SYN4. However, the agglomeration force is stronger for SYN1 and SYN2 particles that lead to secondary particles, which may composed of more than two crystallites.

Literature data showed that the optimal size range of TiO_2 for achieving better photocatalysis was about 25−30 nm on organic compound removal for the aqueous phase,[36] while it was 13 nm in the gas-phase destruction of acetone to form CO_2.[5] Therefore, if one considers the effect of particle size only, then SYN3 and SYN4 particles with an optimal size of around 25 nm should have better activities than SYN1 and SYN2, which have larger secondary sizes of around 50 nm. However, this did not happen in this study. Hence one can conclude that the secondary particle size effect on the photocatalytic activity is not an influential factor on the photoactivity in this study. This could be because the crystallite sizes of SYN1−SYN4 are about the same around 22 nm as calculated by the Scherrer equation.

4.3. Crystal Phase. The crystal phase of photocatalytic particles was determined with the XRPD pattern shown in Figure 5. The XRPD peaks around 25°, 38°, 48°, 55°, and 63° corresponding to anatase crystal are observed for all synthesized tests, with the most significant peak around 25°.

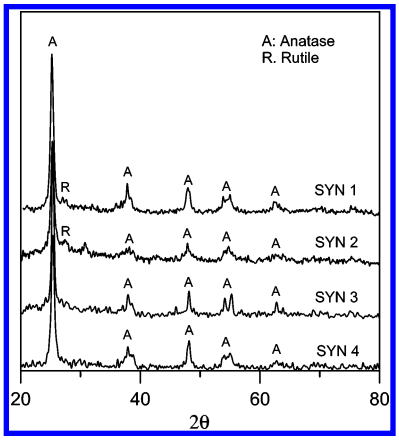

Figure 5. XRPD patterns of photocatalytic particles synthesized in this study.

There is one minor peak at 27.5° (corresponding to rutile crystal) appearing for the product particles of SYN1 and SYN2. The SYN1 and SYN2 photocatalysts were both obtained at the same plasma conditions and the same annealing temperature of 500 °C. The phase transformation of the nanocrystal from anatase to rutile should appear at temperatures higher than 600 °C.[37] However, it is also possible to occur at a lower temperature for N-doped photocatalysts.[8] Since there was only a very small fraction of rutile phase for SYN1 and SYN2 photocatalysts, which may be even within the error range of detection compared to the anatase phase, it is concluded that the crystal phase should have minimal effect on the photocatalytic activity.

4.4. UV−Visible Spectra. Figure 6 shows the Kubelka−Munk absorption unit spectra of the synthesized photocatalysts obtained under different processes of SYN1−SYN4. The absorption edge around 400 nm is assigned to the pure TiO_2 and appears for all processes. On the other hand, a second absorption edge around 520 nm appears only for SYN1and SYN2 and it should be due to the presence of N-doped TiO_2. Although SYN4 was synthesized under N_2/O_2 gas plasma, there

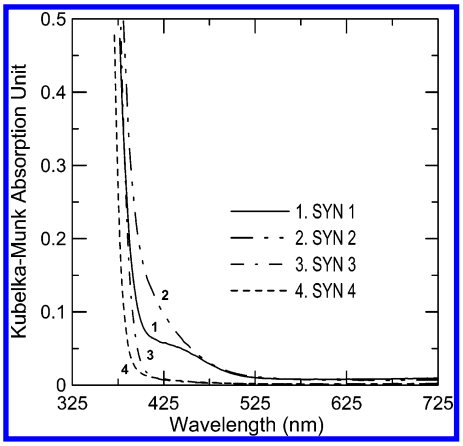

Figure 6. Kubelka−Munk absorption spectra of N-doped photocatalysts synthesized in this study.

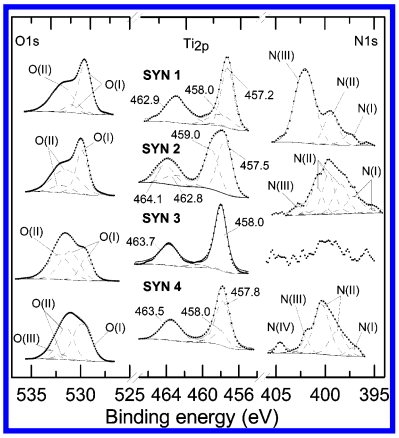

Figure 7. XPS patterns of O 1s, Ti 2p, and N 1s spectra for photocatalytic particles produced in this study. The spectra shown from top to bottom are for SYN1−SYN4 photocatalysts. The dotted lines are XPS measured spectra, while the dashed lines are the fittings of possible binding energy spectra to the XPS data, and the solid lines are the sum of the fitted data.

is no obvious absorption edge in the visible light region. However, although SYN4 photocatalyst did not cause an obvious shift of the absorption edge in the UV−vis absorption spectra, it still showed a visible light photocatalytic effect as shown above in Figure 2 due to the surface absorption or the oxygen vacancy.[24,34]

4.5. Core Level Binding Energy. To prevent the influences of other factors such as crystallite size and particle size of TiO_2 as well as its crystal phase on the photocatalytic activity, the photocatalysts were prepared under the same operating conditions in the APPENS reactor as shown previously. Thus the remaining important factor in the photocatalytic activity is the N-doping status of the photocatalysts.

The XPS spectra of Ti 2p, N 1s, and O 1s for the photocatalytic particles synthesized in this study are shown in Figure 7. One can observe in the middle spectra of Figure 7 that the core level binding energies of Ti 2p under different synthesized tests are around 457.0−459.0 eV for Ti $2p_{3/2}$ and 463.0−464.0 eV for Ti $2p_{1/2}$. Compared to the peak values listed in Table 1, the peaks at 458.0 eV for Ti $2p_{3/2}$ and 463.7 eV for Ti $2p_{1/2}$ are assigned to TiO_2,[25−27,29,31] which can be clearly seen for SYN3 photocatalyst. On the other hand, the presence of TiN (Ti $2p_{3/2}$, 455.2−456.0 eV) and $TiO_{2-x}N_x$ (Ti $2p_{3/2}$, 456.0−459.0 eV) tends to shift the TiO_2 peaks to lower binding energy.[12,25−27,29,31] It was observed that SYN1 photocatalyst has the most significant shift toward lower binding energy of 457.2 eV at Ti $2p_{3/2}$.

The most significant peak of N 1s (right spectra in Figure 7) for SYN1 photocatalyst is observed around 402.9 eV (N(III)), while the most significant N 1s peaks for SYN2 and SYN4 are both located around 398.5−400.8 eV (N(II)). On the other hand, there is no obvious N 1s peak for SYN3 photocatalyst since it was produced without the presence of a nitrogen source.

The major O 1s peaks (left spectra in Figure 7) for SYN1 and SYN2 photocatalysts are both observed around 529.7 ± 2 eV (O(I)), while the major O 1s peaks for SYN3 and SYN4 photocatalyst are both located around 532.0 ± 2 eV (O(II)). One can see from Table 1 that the presence of O(I) peaks indicates that O atoms exist as metal oxides such as TiO_2, while the O(II) and O(III) peaks reveal that the O atoms could exist as oxynitride or other dopants such as CO and OH, or simply as adsorbed O_2. Because there was no nitrogen source in the SYN3 process, for SYN3 photocatalyst the O atoms may exist as CO or appear as adsorbed O_2.

4.6. N-Doped Status of the TiO_2 Photocatalysts. The different N-doping structures in the TiO_2 particles can be seen more clearly by the cross comparison between N 1s and O 1s spectra as shown in Figure 8. The peaks of N(I) observed around 395.8−397.8 eV indicate the possible presence of TiN. They may also indicate the presence of TiN_XO_Y with the simultaneous appearance of O(I) at 531.0 eV.[29] Both the TiN and TiN_XO_Y peaks represent the N substitution for the O in TiO_2.[4,8] TiN was observed in SYN1, SYN2, and SYN4 photocatalysts.

The N(II) peaks located at the region of 398.8−401.2 eV indicates the possible presence of chemisorbed oxynitride with the simultaneous appearance of the O(II) peak around 531.4−532.4 eV. The N(II) peak may be the Ti−(NO) structure[14,16,18] or impurities doped in the interstitial of TiO_2 matrixes.[8,20] The above N-doped statuses are all denoted Ti−(NO) in this study. It was observed in SYN1, SYN2, and SYN4 photocatalysts.

The N(III) peaks located around 402.0−403.0 eV correspond to the oxidized form of TiN into O_X−Ti−N_Y as confirmed by the feature of the O(II) peak at 531.9 eV.[16,21,25] O_X−Ti−N_Y was observed in SYN1, SYN2, and SYN4 photocatalysts. Finally, the N(IV) peak located around 404.6 eV should be Ti−(NO_2)[26,31,32] with a cross comparison of the O(III) peak at 532.2 eV; it appeared only for SYN4 photocatalyst.

Figure 8 also shows the percentage of total N relative to the Ti atomic ratio (denoted N_{total}/Ti in Figure 8) as well as each type of N-doping relative to the total N-doping quantity (N/N_{total}). One can see that the N-doped TiO_2 obtained from SYN2 has the highest N_{total}/Ti atomic ratio of 69%. This is much higher than that of the SYN1 photocatalyst, which has an N_{total}/Ti atomic ratio of only 24%. However, the SYN1 photocatalyst still has a higher photocatalytic activity than the SYN2 photocatalyst. Therefore, one knows that the total quantity of nitrogen in the photocatalyst may not have a direct influence on the visible light photocatalysis. On the other hand, the N-doping status may have a deterministic effect on the photocatalytic activity.

The major type of N-doping for SYN1 is O_X−Ti−N_Y, which accounts for 69.2% of the total N in the photocatalyst. There is also 21.2% Ti−(NO) and only 9.6% TiN observed for SYN1 photocatalyst. On the other hand, for SYN2 photocatalyst, Ti−(NO) is the most significant N-doping (70.2%) and TiN is the secondary doping (22.8%). Also a few percentage O_X−Ti−N_Y appears in SYN2 photocatalyst. The N-doping status for SYN4 photocatalyst is very similar to that of SYN2, with the major peak as Ti−(NO) and minor peaks as O_X−Ti−N_Y and TiN. However, the SYN4 photocatalyst has an additional peak of Ti−NO_2. Besides, its TiN percentage is less than that of SYN2

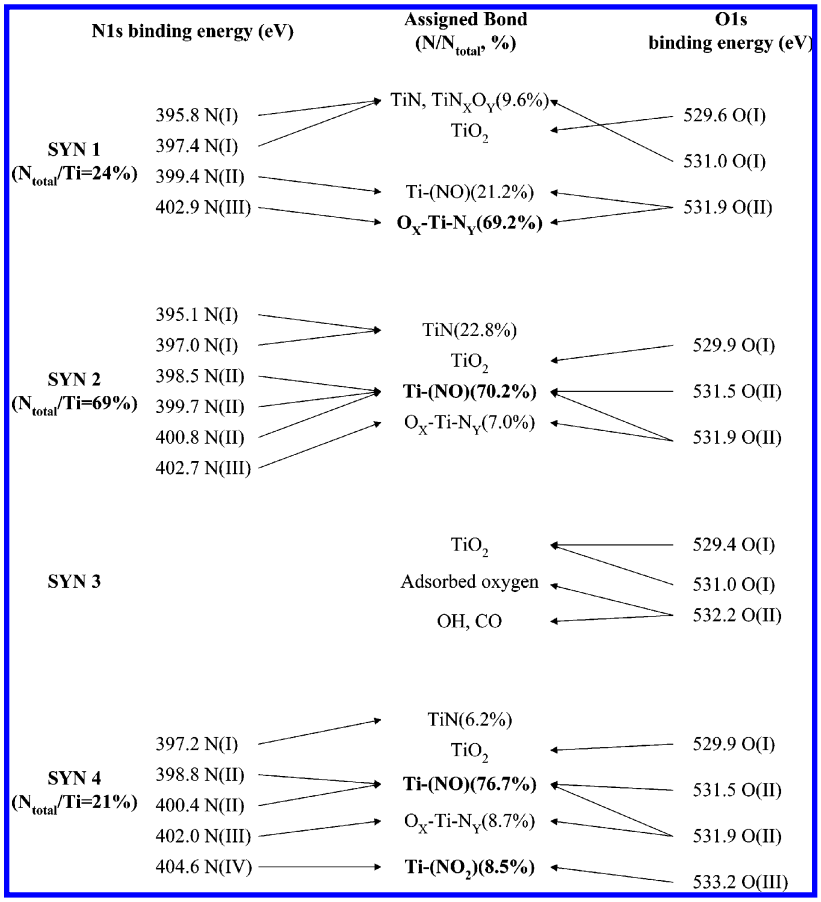

Figure 8. Nitrogen-doping status for SYN1−SYN4 synthesized photocatalysts based on cross comparison of N 1s and O 1s binding energies.

photocatalyst. It was also noted that the TiN located around 395−396 eV only appears for photocatalysts produced by the nitrogen plasma process (SYN1 and SYN2), while the TiN peak located around 397 eV appears for SYN1, SYN2, and SYN4 photocatalysts.

By comparing the XPS results to the photoactivity results shown above in Figure 2, one can suggest that Ti−N, O_X−Ti−N_Y, and Ti−(NO) doped TiO_2 photocatalysts have positive effects on the visible light photocatalysis, and thus the IPA removal efficiencies are higher with SYN1 and SYN2 photocatalysts. This result is similar to those of Sato et al.,[14] Yin et al.,[15] and Diwald et al.,[20] but opposite that of Nosaka et al.[13] The opposite results between these studies are probably because the N-induced localized state[25−27] causes a positive effect on the visible light photocatalysis as oberved in Sato et al.,[14] Yin et al.,[15] Diwald et al.,[20] and this study. However, the photocatalyst prepared by Nosaka et al.[13] could only absorb −(NO) on the catalyst surface and this resulted in a negative effect. However, it requires further study to confirm this hypothesis.

The photocatalytic activity of O_X−Ti−N_Y may be superior to that of Ti−(NO) doped photocatalysts since O_X−Ti−N_Y is the major N-doping for SYN1 photocatalyst. This is in accord with the studies of Chen et al.[16,21] that O_X−Ti−N_Y is an effective dopant. The results indicated, that in addition to the widely accepted Ti−N dopant, both Ti−NO and O_X−Ti−N_Y types of N-doping TiO_2 have positive effects on the visible light photocatalysis.

On the other hand, although SYN4 also showed the presence of Ti−(NO) as a major peak and O_X−Ti−N_Y and TiN as minor peaks, its photoactivity is much less than those of the SYN1 and SYN2 photocatalysts and even worse than that of the pure anatase TiO_2 made by SYN3. This may be caused by the presence of Ti−(NO_2) doping as observed only for SYN4. Therefore, one can suggest that Ti−(NO_2) doping tends have a negative effect on the visible light photocatalysis.

5. Conclusion

Nitrogen-doped TiO_2 was produced by the APPENS process via different plasma and annealing gas compositions. The different binding energies of Ti 2p, N 1s, and O 1s obtained in this study via XPS analysis were grouped into several ranges as TiO_2 and TiN at $2p_{3/2}$ and $2p_{1/2}$, N(I)−N(IV) for N 1s, and O(I)−O(III) for O 1s based on the literature data on N-doped TiO_2 photocatalysts. The N-doping status of TiN, Ti−(NO), O_X−Ti−N_Y, or Ti−(NO_2) was confirmed by the cross comparison of chemical shifts in the binding energies of N, Ti, and O. It was found that Ti−(NO) and O_X−Ti−N_Y are the most significant structures of the N-doped TiO_2 for the N_2 plasma processes. Ti−(NO_2) may form under the presence of both O_2 and N_2 plasma gases. Results on the photocatalytic activities in terms of IPA conversion indicated that, in addition to the widely accepted TiN doping, both Ti−(NO) and O_X−Ti−N_Y types of N-doping TiO_2 have positive effects, but the presence of Ti−(NO_2) tends to have a negative effect on the visible light photocatalysis.

Although the chemical structures of N dopants in the TiO_2 photocatalysts have been speculated in this study and their correlations with the photoactivity have been suggested, further work might still be necessary since there are several types of N dopants present in one photocatalyst. Besides, the actual coordination of the N impurity cannot be identified by the XPS data. Furthermore, Livraghi et al.[24] indicated that some of the N-induced defects are also responsible for the increased photoactivity. Therefore, the simultaneous consideration of all possible

factors for the photoactivity might be required. The production of a pure N speciation in each photocatalyst to directly identify the N-dopant effect on the photocatalytic activity may be a challenging work in the future.

Acknowledgment. This study was supported by the National Science Council, Taiwan, through Grants NSC 92-2211-E-009-017 and NSC 93-2211-E-009-018.

References and Notes

(1) Fujishima, A.; Rao, T. N.; Tryk, D. A. *J. Photochem. Photobiol., C* **2000**, *1*, 1.

(2) Umebayashi, T.; Yamaki, T.; Yamamoto, S.; Miyashita, A.; Tanaka, S.; Sumita, T.; Asai, K. *J. Appl. Phys.* **2003**, *93*, 5156.

(3) Wang, Z. M.; Yang, G.; Biswas, P.; Bresser, W.; Boolchand, P. *Powder Technol.* **2001**, *114*, 197.

(4) Asahi, R.; Morikawa, T.; Ohwaki, T.; Aoki, K.; Taga, Y. *Science* **2001**, *293*, 269.

(5) Ihara, T.; Miyoshi, M.; Iriyama, Y.; Matsumoto, M.; Sugihara, S. *Appl. Catal., B* **2003**, *42*, 403.

(6) Irie, H.; Watanabe, Y.; Hashimoto, K. *J. Phys. Chem. B* **2003**, *107*, 5483.

(7) Wawrzyniak, B.; Morawski, A. W. *Appl. Catal., B* **2006**, *62*, 150.

(8) Maeda, M.; Watanabe, T. *J. Electrochem. Soc.* **2006**, *153* (3), C186.

(9) Yin, S.; Ihara, K.; Aita, Y.; Komatsu, M.; Sato, T. *J. Photochem. Photobiol., A* **2006**, *179*, 105.

(10) Miao, L.; Tanemura, S.; Watanabe, H.; Mori, Y.; Kaneko, K.; Toh, S.; *J. Cryst. Growth* **2004**, *260*, 118.

(11) Suda, Y.; Kawasaki, H.; Ueda, T.; Ohshima, T. *Thin Solid Films* **2005**, *475*, 337.

(12) Yang, T.-S.; Shiu, C.-B.; Wong, M.-S. *Surf. Sci.* **2004**, *548*, 75.

(13) Nosaka, Y.; Matsushita, M.; Nishino, J.; Nosaka, A. Y. *Sci. Technol. Adv. Mater*. **2005**, *6*, 143.

(14) Sato, S.; Nakamura, R.; Abe, S. *Appl. Catal., A* **2005**, *284*, 131.

(15) Yin, S.; Aita, Y.; Komatsu, M.; Wang, J.; Tang, Q.; Sato, T. *J. Mater. Chem.* **2005**, *15*, 674.

(16) Chen, X.; Lou, Y.; Samia, A. C. S.; Burda, C.; Gole, J. L. *Adv. Funct. Mater*. **2005**, *15*, 41.

(17) Livraghi, S. Votta, A.; Paganini, M. C.; Giamello, E. *Chem. Commun.* **2005**, 498.

(18) Gyorgy, E.; Perez del Pino, A.; Serra, P.; Morenza, J. L. *Surf. Coat. Technol.* **2003**, *173*, 265.

(19) Bai, H.; Chen, C.; Lin, C.; Den, W.; Chang, C. L. *Ind. Eng. Chem. Res.* **2004**, *43*, 7200.

(20) Diwald, O.; Thompson, T. L.; Zubkov, T.; Goralski, Ed. G.; Walck, S. D.; Yates, J. T., Jr. *J. Phys. Chem. B* **2004**, *108*, 6004.

(21) Chen, X.; Burda, C. *J. Phys. Chem. B* **2004**, *108*, 15446.

(22) Di Valentin, C.; Pacchioni, G.; Selloni, A. *Phys. Rev. B* **2004**, *70*, 085116.

(23) Di Valentin, C.; Pacchioni, G.; Selloni, A.; Livraghi, S.; Giamello, E. *J. Phys. Chem. B* **2005**, *109* (23), 11414.

(24) Livraghi, S.; Paganini, M. C.; Giamello, E.; Selloni, A.; Di Valentin, C.; Pacchioni, G. *J. Am. Chem. Soc.* **2006**, *128*, 15666.

(25) Esaka, F.; Furuya, K.; Shimada, H.; Imamura, M.; Matsubayashi, N.; Sato, H.; Nishijima, A.; Kawana, A.; Ichimura, H.; Kikuchi, T. *J. Vac. Sci. Technol., A* **1997**, *15* (5), 2521.

(26) *Handbook of X-ray Photoelectron Spectroscopy*; Jill, C., Ed.; Perkin-Elmer Corp.: Waltham, MA, 1992; pp 41−73.

(27) Saha, N. C.; Tompkins, H. G. *J. Appl. Phys.* **1992**, *72* (7), 3072.

(28) Battiston, G. A.; Gerbasi, R.; Gregori, A.; Porchia, M.; Cattarin, S.; Rizzi, G. A. *Thin Solid Films* **2000**, *371*, 126.

(29) Guillot, J.; Jouaiti, A.; Imhoff, L.; Domenichini, B.; Heintz, O.; Zerkout, S.; Mosser, A.; Bourgeois, S. *Surf. Interface Anal.* **2002**, *34*, 577.

(30) Wu, H. Z.; Chou, T. C.; Mishra, A.; Anderson, D. R.; Lampert, J. K.; Gujrathi, S. C. *Thin Solid Films* **1990**, *191*, 55.

(31) Lu, F.-H.; Feng, S.-P.; Chen, H.-Y.; Li, J.-K. *Thin Solid Films* **2000**, *375*, 123.

(32) Rodriguez, J. A.; Jirsak, T.; Dvorak, J.; Sambasivan, S.; Fischer, D. *J. Phys. Chem. B* **2000**, *104*, 319.

(33) Jirsak, T.; Dvorak, J.; Rodriguez, J. A. *Surf. Sci.* **1999**, *436*, L683.

(34) Huang, C.-M.; Chen, L.-C.; Cheng, K.-W, Pan, G.-T. *J. Mol. Catal. A* **2007**, *261*, 218.

(35) Musić, S.; Gotić, M.; Ivanda, M.; Popović, S.; Turković, A.; Trojko, R.; Sekulić, A.; Furić, K. *Mater. Sci. Eng., B* **1997**, *47*, 33.

(36) Almquist, C. B.; Biswas, P. *J. Catal.* **2002**, *212*, 145.

(37) Zhang, H.; Banfield, J. F. *J. Mater. Res.* **2000**, *15*, 437.